

Collective modes of spin-orbit coupled Fermi gases in the repulsive regime

Shang-Shun Zhang¹, Xiao-Lu Yu¹, Jinwu Ye^{2,3}, and Wu-Ming Liu¹

¹*Beijing National Laboratory for Condensed Matter Physics,*

Institute of Physics, Chinese Academy of Sciences, Beijing 100190, China

²*Department of Physics and Astronomy, Mississippi State University, MS 39762, USA*

³*Key Laboratory of Terahertz Optoelectronics, Ministry of Education,*

Department of Physics, Capital Normal University, Beijing 100048, China

(Dated: February 13, 2013)

We investigate the collective modes in the spin-orbit coupled Fermi gas with repulsive s -wave interaction. The interplay between spin-orbit coupling and atom-atom interactions plays the crucial role in the collective behaviors of Fermi gas. In contrast with ordinary Fermi liquid, spin-orbit coupled Fermi gas has strongly correlated spin and density excitations. Within the scheme of random phase approximation, we classify collective modes based on the symmetry group and determine their properties via the poles of corresponding correlation functions. Besides, the particle-hole continuum is obtained, where the imaginary part of these correlation functions become non-vanishing. We make comparisons with collective excitations in the ordinary Fermi liquid without spin-orbit coupling and in a helical liquid, i.e., surface states of a three dimensional topological insulator. We also propose an experimental protocol for detecting these collective modes and discuss corresponding experimental signatures in the ultracold Fermi gases experiment.

PACS numbers: 03.75.Ss, 03.75.Kk, 67.85.Lm

I. INTRODUCTION

A great deal of attentions have been focused on the spin-orbit coupling (SOC) because of its fundamental interests in condensed matter systems [1–6] and important applications in spintronic device [7]. In recent years, a wide range of atomic physics and quantum optics technology provides unprecedented manipulation of a variety of intriguing quantum phenomena, therefore it seems to provide an ideal platform to study the effects of SOC in ultracold atomic systems. The experimental studies on this topic have made great breakthrough. Based on the Berry phase effect [8] and its non-Abelian generalization [9], Spielman's group in NIST has successfully generated a synthetic external Abelian or non-Abelian gauge potential coupled to neutral atoms [10–13]. Recently, the SOC Fermi gas has been first engineered in weakly repulsive ⁴⁰K [14] or ⁶Li [15] atomic gases. Realization of SOC in quantum gases will open a whole new avenue in cold atom physics.

Motivated by these recent experimental progresses of ultracold Fermi gases, we consider the two dimensional (2D) Fermi gas with SOC in the repulsive regime. The repulsive atom-atom interaction can be engineered in the upper branch of energy spectrum, where there are uncondensed Fermi gas in the absence of molecule formation [16]. The repulsive Fermi gas is stable when it is far away from the resonant regime, which has been successfully reached in experiment [17]. In our previous work, we have studied low energy single particle excitations and calculated the Fermi liquid parameters such as the quasi-particle lifetime, renormalization factor and the effective mass in the repulsive regime [18].

In this paper, we investigate the collective modes of two dimensional Fermi gas with SOC in the repulsive regime.

The research of the low energy collective modes in degenerated quantum gases yields a wealth of insights into the properties of ultracold atomic systems. A lot of previous studies have devoted to the collective behaviors in various symmetry broken phases of ultracold atomic systems, which include the degenerate gas at the Bose-Einstein condensation (BEC) to Bardeen-Cooper-Schrieffer (BCS) crossover [19–22], Fermi gas in the unitarity limit [23–26], imbalanced Fermi gas [27], and BEC in the presence of SOC [28, 29]. By contrast, we focus on the normal state regime of the SOC Fermi gas in this work. The interplay between SOC and s -wave atom-atom interactions plays the crucial role in our investigation. Compared with ordinary Fermi gas, SOC Fermi gas has strongly correlated spin and density excitations. Within the scheme of random phase approximation (RPA), we classify all the collective modes and determine their properties via the poles of corresponding RPA correlation functions.

In contrast with previous works in solid state systems, the consideration of s -wave interaction in ultracold atomic systems instead of the Coulomb interaction leads to qualitatively different collective behaviors. The reasons for this are twofold: First, the force range of the s -wave interaction is short and the interaction vertex is independent to the momentum transfer. Second, the s -wave interaction is spin-dependent in ultracold Fermi gas, which can be decomposed into the density and spin channels [30]. The collective modes of this system are grouped into two categories: (i) one branch of gapless mode, namely zero sound, which is an oscillation of density coupled with the transverse spin oscillation; (ii) three branches of gapped modes. We expect our microscopic calculations of the collective modes would have immediate applications to the SOC Fermi gas in the upper branch of the energy spectrum.

The paper is organized as follows. The model building

of SOC Fermi gas with repulsive s -wave interaction is described in Sec. II, where all the microscopic parameters and the helicity eigenstates are explained. Furthermore, the collective modes are classified based on the symmetric property. In Sec. III, we develop a general approach to calculate a series of RPA correlations functions. In Sec. IV, we investigate the solutions of matrix forms of RPA equation analytically and numerically. In Sec. V, we provide a comparison and discussion of the collective modes in various fermionic systems. Finally, we propose an experiment protocol to detect collective modes in Fermi gas with SOC on the upper branch of energy spectrum and estimate corresponding experimental signatures in Sec. VI.

II. THE SOC FERMION GAS WITH REPULSIVE S -WAVE SCATTERING

We consider the collective modes of a 2D spin-1/2 ultracold repulsive Fermi gas with Rashba SOC, described by the model Hamiltonian,

$$\mathcal{H} = \sum_{\mathbf{k}, \alpha, \beta} c_{\mathbf{k}, \alpha}^\dagger h_{\alpha\beta} c_{\mathbf{k}, \beta} + 2g \sum_{\mathbf{k}, \mathbf{p}, \mathbf{q}} c_{\mathbf{k}+\mathbf{q}, \uparrow}^\dagger c_{\mathbf{p}-\mathbf{q}, \downarrow}^\dagger c_{\mathbf{p}, \downarrow} c_{\mathbf{k}, \uparrow}, \quad (1)$$

where α and β are the spin indexes. The first part is the non-interacting Hamiltonian, and h is the single particle Hamiltonian with SOC

$$h = \frac{\mathbf{k}^2}{2m} + \lambda(\hat{\mathbf{z}} \times \mathbf{k}) \cdot \boldsymbol{\sigma} - \mu, \quad (2)$$

where $\mu = k_F^2/2m$ is the chemical potential and k_F is the Fermi momentum in the absence of SOC, λ represents the strength of SOC. Here and bellow, \hbar is taken as 1. The eigenstates of single particle Hamiltonian h can be obtained as follows

$$|\mathbf{k}, \pm 1\rangle = \frac{1}{\sqrt{2}} \begin{pmatrix} 1 \\ \pm i e^{i\phi(\mathbf{k})} \end{pmatrix}, \quad (3)$$

where $\phi(\mathbf{k}) = \arctan(k_y/k_x)$ is the azimuthal angle of momentum \mathbf{k} and the helicity ± 1 represents that the in-plane spin polarization is right-handed or left-handed with respect to the momentum. Hence the eigenstates in Eq. (3) are naturally called helicity bases. The dispersion relations for two helicity bases are $\xi_{\mathbf{k}, \pm} = (\mathbf{k}^2 \pm 2k_R|\mathbf{k}| - k_F^2)/2m$, where $k_R = m\lambda$ corresponds to the recoil momentum in experiments [14, 15]. The Fermi momentum and the recoil momentum provide two scales for the 2D Fermi gas with SOC, and the dimensionless ratio of them $\gamma = k_R/k_F$ denotes the significance of SOC. The Fermi surfaces are given by $\xi_{\mathbf{k}, s} = 0$, which gives rise to two circles in the momentum space with two Fermi momenta as $k_s = \kappa k_F - s k_R$, where $\kappa = \sqrt{1 + \gamma^2}$. We plot the energy spectrum and the Fermi surfaces with the associated spin textures in Fig. 1 for two different chemical potentials. We note that the outer and inner

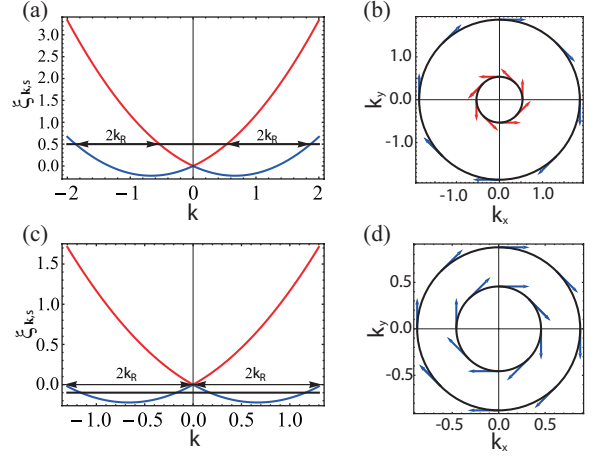


FIG. 1. (Color online) (a) and (c) plot the energy spectrum in presence of spin-orbit coupling with different fillings. The thick black horizontal line denotes the level of chemical potential. (b) and (d) show the Fermi surfaces and the associated spin textures corresponding to (a) and (c) respectively.

Fermi surfaces shown in Fig. 1 (b) have two opposite helicity, and therefore one has Berry phase π , another $-\pi$. While the outer and inner Fermi surfaces shown in Fig. 1 (d) have the same helicity, and therefore the Berry phase π and π respectively. The system experiences Lifshitz transitions when the chemical potential passes the Dirac point of the spectrum at $\mathbf{k} = 0$ [31, 32]. In the present work, we only consider the case shown in Fig. 1 (a), where the two Fermi surfaces correspond to different helicity bands.

The second term in Eq. (1) represents the s -wave interaction in ultracold atomic gases. The low energy interaction among ultracold atoms is universally determined by the scattering length a_s [33–35]. For quasi-2D system, which can be realized through a strong confinement in the $\hat{\mathbf{z}}$ direction perpendicular to the 2D plane, the effective s -wave scattering strength is determined by $2g = 4\pi N a_s / 3\sqrt{2\pi} m \zeta_z$, where N is the total atom number, m is the mass for atom, and $\zeta_z = \sqrt{1/m\omega_z}$ is the confinement length of the atomic gases along $\hat{\mathbf{z}}$ direction with ω_z as the trap frequency of the confinement potential. The significance of s -wave interaction in ultracold atoms could be characterized by the dimensionless ratio of the average interaction energy and kinetic energy $\varepsilon_{int}/\varepsilon_{kin}$, which equals $mg = 2\pi N a_s / 3\sqrt{2\pi} m \zeta_z$. With the technique of Feshbach resonance, the strength of the repulsive interaction can be tuned within a wide range [36–41].

The dynamical response of SOC Fermi gas can be described via the density and spin susceptibility

$$\chi^{\mu\nu}(\mathbf{q}, i\omega_m) = \sum_{\mathbf{k}, \mathbf{p}} \sum_{\alpha\beta\gamma\delta} \int_0^\beta d\tau e^{i\omega_m\tau} \langle \mathcal{T}_\tau c_{\mathbf{k}\alpha}^\dagger \sigma_{\alpha\beta}^\mu c_{\mathbf{k}+\mathbf{q}\beta}(\tau) \times c_{\mathbf{p}+\mathbf{q}\gamma}^\dagger \sigma_{\gamma\delta}^\nu c_{\mathbf{p}\delta}(0) \rangle, \quad (4)$$

where $\sigma^\mu = (\sigma^0, \boldsymbol{\sigma})$. We could study the collective modes through the poles of the dynamical response function to external density and spin perturbations. The SOC is isotropic in the 2D x - y plane. The density and spin susceptibility $\chi^{\mu\nu}$ is invariant under the simultaneous rotation of the momentum \mathbf{q} and the spin $\mathbf{s} = \frac{1}{2}\boldsymbol{\sigma}$ around the $\hat{\mathbf{z}}$ axis, namely the rotation group: $SO(2)_{\mathcal{D}}$, where the subscript \mathcal{D} represents the combined operation for the momentum and spin space.

Furthermore, considering the Rashba-type SOC and the rotation invariance of Fermi surface around the $\hat{\mathbf{z}}$ axis, the density excitations are coupled with the transverse components of the spin excitations $s^T \equiv (\hat{\mathbf{z}} \times \hat{\mathbf{q}}) \cdot \mathbf{s}$ intrinsically, while both of them are decoupled from the longitudinal component $s^L \equiv \hat{\mathbf{q}} \cdot \mathbf{s}$ and perpendicular component $s^Z \equiv \hat{\mathbf{z}} \cdot \mathbf{s}$ [42]. Therefore, it is convenient to study the collective modes under the helical spin bases, which is defined as $\{n, s^T, s^L, s^Z\}$ with n as the density component. Under the helical spin bases, the 4×4 susceptibility matrix decomposes into two 2×2 matrices. One is in the subspace of n - s^T , and the other is in the subspace of s^L - s^Z . Based on this decomposition of the susceptibility, the collective modes are grouped into two categories: one with the density and transverse spin excitations s^T , and the others with the perpendicular and longitudinal spin excitations s^Z, s^L . Without loss of generality, we can assume $\mathbf{q} = q\mathbf{e}_x$ in the following. Thus we have

$$s^T = s^y, s^L = s^x, s^Z = s^z. \quad (5)$$

In the following sections, we will work in this representation to calculate the density and spin susceptibility and investigate the collective modes of SOC Fermi gas.

III. DENSITY AND SPIN CORRELATION FUNCTIONS

A. Feynman Rules and Susceptibilities

The particle line shown in Fig. 2 (a) represents the Green's function with SOC in the Matsubara formalism

$$G_{\alpha\beta}^0(\mathbf{k}, ik_n) = \sum_{s=\pm 1} \frac{(P_s)_{\alpha\beta}}{ik_n - \xi_{\mathbf{k},s}}, \quad (6)$$

where $ik_n = (2n+1)\pi k_B T$ is the fermionic Matsubara frequency and P_s is the projection operator to the helicity eigenstates: $P_s = [1 + s(\hat{\mathbf{z}} \times \hat{\mathbf{k}}) \cdot \boldsymbol{\sigma}]/2$. It is helpful to apply the Fierz identity $2\epsilon^{\delta\gamma}\epsilon^{\alpha\beta} = (\sigma^\mu)^{\beta\gamma}(\sigma_\mu)^{\alpha\delta}$ to the s -wave interaction vertex, where $\sigma^\mu = (\sigma^0, \boldsymbol{\sigma})$ and $\sigma_\mu = (\sigma^0, -\boldsymbol{\sigma})$. The interacting part can be rewritten as

$$V = \frac{1}{2!2!} \sum_{\alpha\beta\gamma\delta} \sum_{\mathbf{k}, \mathbf{p}, \mathbf{q}} V_{\alpha\delta, \beta\gamma} c_\delta^\dagger(\mathbf{k} + \mathbf{q}) c_\gamma^\dagger(\mathbf{p} - \mathbf{q}) c_\beta(\mathbf{p}) c_\alpha(\mathbf{k}), \quad (7)$$

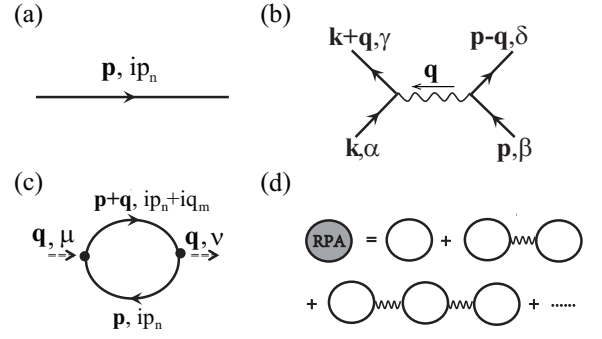


FIG. 2. (Color online) (a) The free Green's function with SOC: $-G^0(\mathbf{p}, ip_n)$. (b) The interaction vertex $-g(\sigma^\mu)^{\beta\gamma}(\sigma_\mu)^{\alpha\delta}$. (c) One bubble diagram: the bare susceptibility $\chi^{\mu\nu}(\mathbf{q}, iq_m)$. (d) The sum of the bubble diagrams gives the RPA susceptibility $\chi_{RPA}^{\mu\nu}(\mathbf{q}, iq_m)$.

where $V_{\alpha\delta, \beta\gamma} = g(\sigma^\mu)_{\beta\gamma}(\sigma_\mu)_{\alpha\delta}$. The Feynman rule for the interaction vertex is shown in Fig. 2 (b). In fact, the interaction vertex considered here includes two cases: $(\mathbf{k} \uparrow, \mathbf{p} \downarrow) \rightarrow (\mathbf{k}' \uparrow, \mathbf{p}' \downarrow)$ and $(\mathbf{k} \uparrow, \mathbf{p} \downarrow) \rightarrow (\mathbf{k}' \downarrow, \mathbf{p}' \uparrow)$. It's important to notice that the infinite summation with this interaction vertex actually include both bubble and ladder diagrams [43].

The collective modes and particle-hole pairs are two fundamental types of excitations of the SOC Fermi gas. The dispersions of collective modes are determined by the poles of the density and spin susceptibility. With these Feynman rules defined above, the RPA susceptibility can be evaluated as (see Fig. 2 (d))

$$\chi_{RPA}^{\mu\nu}(\mathbf{q}, iq_m) = \chi^{\mu\rho}(\mathbf{q}, iq_m) \left(\frac{1}{1 + g\eta\chi(\mathbf{q}, iq_m)} \right)^{\rho\nu}, \quad (8)$$

where

$$\eta = \text{diag}\{1, -1, -1, -1\}, \quad (9)$$

and χ is the bare susceptibility for noninteracting Hamiltonian.

In Matsubara formalism, the bare susceptibility $\chi^{\mu\nu}(\mathbf{q}, iq_m)$ is given by the one loop diagram as shown in Fig. 2 (c)

$$\chi^{\mu\nu}(\mathbf{q}, iq_m) = -k_B T \sum_{\mathbf{k}, ik_n} \text{Tr}[G^0(\mathbf{k} + \mathbf{q}/2, ip_n) \sigma_\mu \times G^0(\mathbf{k} - \mathbf{q}/2, ik_n - iq_m) \sigma_\nu], \quad (10)$$

where $iq_m = 2m\pi k_B T$ and $ik_n = (2n+1)\pi k_B T$ are the bosonic and fermionic Matsubara frequencies, respectively. The Green's function $G^0(\mathbf{k}, ik_n)$ includes a momentum-dependent projection operator P_s , and the trace in Eq. (10) gives rise to an overlap factor as

$$F_{sr}^{\mu\nu} = \text{Tr}[P_s(\mathbf{k} + \mathbf{q}/2) \sigma^\mu P_r(\mathbf{k} - \mathbf{q}/2) \sigma^\nu], \quad (11)$$

where $\mu, \nu = 0, 1, 2, 3$ represent the density and spin

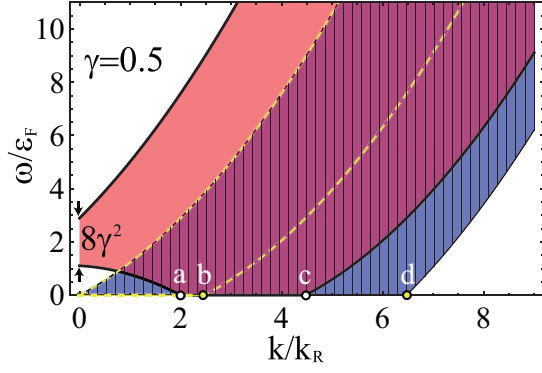


FIG. 3. (Color online) Particle-hole continuum of SOC Fermi gas for $\gamma = 0.5$. The red region surrounded by the thick black lines represents the interband particle-hole continuum. The region surrounded by the dashed yellow lines represents continuum of intraband particle-hole excitations with helicity +1, the blue region filled with vertical lines, with helicity -1. The points a, b, c and d correspond to the momenta $2k_R, 2k_{+1}, 2\kappa k_F$ and $2k_{-1}$ respectively, where the static susceptibility function exhibits singular behaviors [44].

components in $\hat{\mathbf{x}}, \hat{\mathbf{y}}, \hat{\mathbf{z}}$ directions, and s, r are helicity indexes. After summing over the fermionic Matsubara frequency ik_n , and performing the analytical continuation $iq_m \rightarrow \omega + i0^+$, we have

$$\chi^{\mu\nu}(\mathbf{q}, \omega) = - \sum_{\mathbf{k}, s, r} F_{sr}^{\mu\nu} \frac{f(\xi_{\mathbf{k}-\mathbf{q}/2, s}) - f(\xi_{\mathbf{k}+\mathbf{q}/2, r})}{\xi_{\mathbf{k}-\mathbf{q}/2, s} - \xi_{\mathbf{k}+\mathbf{q}/2, r} + \omega + i0^+}. \quad (12)$$

At zero temperature, the Fermi occupation function is $f(\xi) = \Theta(-\xi)$. The numerator in the Eq. (12) is non-zero only if

$$\xi_{\mathbf{k}-\mathbf{q}/2, s} > 0, \quad \xi_{\mathbf{k}+\mathbf{q}/2, r} < 0, \quad (13)$$

or

$$\xi_{\mathbf{k}-\mathbf{q}/2, s} < 0, \quad \xi_{\mathbf{k}+\mathbf{q}/2, r} > 0, \quad (14)$$

which represent the conditions for particle-hole excitations. The $\xi_{\mathbf{k}-\mathbf{q}/2, s} - \xi_{\mathbf{k}+\mathbf{q}/2, r}$ in the denominator is the corresponding particle-hole exciton energy, which includes the contribution from intraband and interband and forms a continuum as shown in Fig. 3. Accordingly, the contributions to the susceptibility come from two aspects: the intraband $r = s$ and the interband $r = -s$. When the frequency and momentum of the susceptibility ω, \mathbf{q} fall in the particle-hole continuum (see Fig. 3), the integration in Eq. (12) will develop a non-zero imaginary part, which corresponds to the damping of the collective excitations. The details about this integration will be further discussed in the following sections and Appendix A. The static density-density susceptibility $\chi^{00}(\mathbf{q})$ exhibits singular behaviors at $|\mathbf{q}| = 2k_R$ and $|\mathbf{q}| = 2\kappa k_F$. In addition, there are weak anomalies at $|\mathbf{q}| = 2k_{+1}$ and

$|\mathbf{q}| = 2k_{-1}$ caused by the intraband virtual transitions [44]. These specific momenta are shown in Fig. 3, which appear as edges of the intra- and inter-band particle-hole excitation continuum.

We want to make some general observations of the overlap factor $F_{sr}^{\mu\nu}$ and bare susceptibility χ as following: (i) $F_{sr}^{\dagger}(\mathbf{q}) = F_{sr}(\mathbf{q})$. (ii) $F_{sr}^{\mu\nu}(\mathbf{q}) = F_{rs}^{\nu\mu}(-\mathbf{q})$. (iii) $\chi(\mathbf{q}, \omega)^{\dagger} = \chi(-\mathbf{q}, -\omega)$. In the long wave length limit $|\mathbf{q}| \rightarrow 0$, the overlap factor $F^{\mu\nu}$ can be expanded relative to \mathbf{q} up to $\mathcal{O}(\mathbf{q}^2)$ approximately. The intraband contribution is

$$F_{s,s}^{\mu\nu} = \begin{pmatrix} 1 & -s \cos \theta & s \sin \theta & i \frac{|\mathbf{q}| \sin \theta}{2|\mathbf{k}|} \\ -s \cos \theta & \cos^2 \theta & -\frac{\sin 2\theta}{2} & -i \frac{s|\mathbf{q}| \sin 2\theta}{4|\mathbf{k}|} \\ s \sin \theta & -\frac{\sin 2\theta}{2} & \sin^2 \theta & i \frac{s|\mathbf{q}| \sin^2 \theta}{2|\mathbf{k}|} \\ -i \frac{|\mathbf{q}| \sin \theta}{2|\mathbf{k}|} & i \frac{s|\mathbf{q}| \sin 2\theta}{4|\mathbf{k}|} & -i \frac{s|\mathbf{q}| \sin^2 \theta}{2|\mathbf{k}|} & 0 \end{pmatrix}, \quad (15)$$

where θ is the azimuthal angle of $\hat{\mathbf{k}} = (\cos \theta, \sin \theta)$. The interband contribution is

$$F_{s,-s}^{\mu\nu} = \begin{pmatrix} 0 & \frac{s|\mathbf{q}| \sin^2 \theta}{2|\mathbf{k}|} & \frac{s|\mathbf{q}| \sin 2\theta}{4|\mathbf{k}|} & -i \frac{|\mathbf{q}| \sin \theta}{2|\mathbf{k}|} \\ \frac{s|\mathbf{q}| \sin^2 \theta}{2|\mathbf{k}|} & \sin^2 \theta & \frac{\sin 2\theta}{2} & -is \sin \theta \\ \frac{s|\mathbf{q}| \sin 2\theta}{4|\mathbf{k}|} & \frac{\sin 2\theta}{2} & \cos^2 \theta & -is \cos \theta \\ i \frac{|\mathbf{q}| \sin \theta}{2|\mathbf{k}|} & is \sin \theta & is \cos \theta & 1 \end{pmatrix}. \quad (16)$$

In the following calculations, we will find that the susceptibility decomposes into two 2×2 matrices, which coincides with the argument in Sec. II. B based on the symmetry property of this system. Besides, the momentum \mathbf{q} dependent terms in the overlap factor have negligible contributions to the low- q (long wave length limit) properties of the collective modes, such as the sound velocity of the gapless mode and the energy gaps of the gapped modes.

B. Intraband contributions ($r = s$)

In the long wave length and low frequency limit ($q \ll k_F, \omega \ll \mu$), the expansions of the particle-hole exciton energy and occupation functions in Eq. (12) to the leading order of $|\mathbf{q}|$ are

$$\xi_{\mathbf{k}-\frac{\mathbf{q}}{2}, s} - \xi_{\mathbf{k}+\frac{\mathbf{q}}{2}, s} \simeq -\frac{k + sk_R}{m} \hat{\mathbf{k}} \cdot \mathbf{q}, \quad (17)$$

and

$$f(\xi_{\mathbf{k}-\frac{\mathbf{q}}{2}, s}) - f(\xi_{\mathbf{k}+\frac{\mathbf{q}}{2}, s}) \simeq -\delta(\xi_{\mathbf{k}, s}) (\xi_{\mathbf{k}-\frac{\mathbf{q}}{2}, s} - \xi_{\mathbf{k}+\frac{\mathbf{q}}{2}, s}). \quad (18)$$

Both have corrections of $\mathcal{O}(q^2/k_F^2)$. The intraband susceptibility reads as

$$\chi^{\mu\nu}(\mathbf{q}, iq_m) = -\frac{m}{4\pi^2 \kappa} \sum_s \frac{k_s}{k_F} \int d\theta F_{ss}^{\mu\nu} \frac{\cos \theta}{y^+ - \cos \theta}, \quad (19)$$

where $y = m\omega/\kappa k_F |\mathbf{q}|$ and θ is the angle between \mathbf{k} and \mathbf{q} . Making use of the overlap factor given in Eq. (15), the elements of $\chi(\mathbf{q}, \omega)$ can be expressed in terms of the following integrals

$$\chi^{\text{intra}}(\mathbf{q}, \omega) = -\frac{m}{\pi} \begin{pmatrix} I_1 & \frac{\gamma}{\kappa} I_2 & 0 & 0 \\ \frac{\gamma}{\kappa} I_2 & I_3 & 0 & 0 \\ 0 & 0 & I_5 & 0 \\ 0 & 0 & 0 & 0 \end{pmatrix}, \quad (20)$$

where the definitions and results of these integrations I_1, I_2, I_3 , and I_5 are given in Appendix A.

C. Interband contributions ($r = -s$)

Similar to the intraband contribution, the energy of the interband particle-hole excitation is expanded relative to \mathbf{q} to the leading order

$$\xi_{\mathbf{k}-\frac{\mathbf{q}}{2}, s} - \xi_{\mathbf{k}+\frac{\mathbf{q}}{2}, -s} \simeq \frac{k}{m} (2sk_R - \hat{\mathbf{k}} \cdot \mathbf{q}), \quad (21)$$

with corrections of $\mathcal{O}(q^2/k_F^2)$. We notice that the energy of interband particle-hole excitation obtains an additional term $\pm 2\kappa k_R/m$ in the presence of SOC. This term dominates the energy of particle-hole excitation at the region $q \ll k_R$, which is dramatically important for giving rise to the low- q properties of the collective excitations, including the sound speed of the gapless modes and the energy gaps of the gapped modes. The difference of occupation is expanded as

$$f(\xi_{\mathbf{k}-\frac{\mathbf{q}}{2}, s}) - f(\xi_{\mathbf{k}+\frac{\mathbf{q}}{2}, -s}) \simeq -s\Theta(k_R - |k - \kappa k_F|) + [\delta(k - k_s) + \delta(k - k_{-s})] \frac{\hat{\mathbf{k}} \cdot \mathbf{q}}{2}. \quad (22)$$

The difference of occupation contains two contributions, which give rise to interband susceptibility: $\chi^{\text{inter}} =$

$\chi_I^{\text{inter}} + \chi_{II}^{\text{inter}}$. The second part is negligible for properties of the collective modes in the low- q regime where $|\mathbf{q}| \ll k_R$.

The first part χ_I^{inter} is an integration within the momentum shell $\kappa k_F - k_R < |\mathbf{k}| < \kappa k_F + k_R$, which can be evaluated straightforwardly for weak SOC with $\gamma \ll 1$

$$\chi_I^{\text{inter}} = \frac{mk_R}{\pi|\mathbf{q}|} \sum_s \begin{pmatrix} 0 & \frac{\gamma|\mathbf{q}|I_4}{2k_R} & 0 & 0 \\ \frac{\gamma|\mathbf{q}|I_4}{2k_R} & s\kappa I_4 & 0 & 0 \\ 0 & 0 & s\kappa I_2 & -i\kappa I_1 \\ 0 & 0 & i\kappa I_1 & s\kappa I_0 \end{pmatrix}. \quad (23)$$

The definitions and results of these integrals I_1, I_2, I_4 are given in Appendix A, and the arguments of them are $y + 2sk_R/|\mathbf{q}|$. The additional term $2sk_R/|\mathbf{q}|$ comes from the split of the energy band. For strong SOC with $\gamma \sim \mathcal{O}(1)$, the evaluation of χ_I^{inter} are simplified in the long wave length regime with $q \ll k_R$

$$\chi_I^{\text{inter}} = \frac{m}{\pi} \sum_s \begin{pmatrix} 0 & 0 & 0 & 0 \\ 0 & F_s/2 & 0 & 0 \\ 0 & 0 & F_s/2 & 0 \\ 0 & 0 & 0 & F_s \end{pmatrix} + \mathcal{O}\left(\frac{\mathbf{q}}{k_R}\right), \quad (24)$$

where $F_s = (2\gamma - z_s \ln \frac{z_s + \kappa + \gamma}{z_s + \kappa - \gamma})/8\gamma$ with $z_s = \omega/4s\gamma\epsilon_F$. It can be shown that Eq. (24) reduces to Eq. (23) to the first order of γ at the low- q regime.

The second part $\chi_{II}^{\text{inter}}(\mathbf{q}, \omega)$ is an integration performed in two separated Fermi surfaces

$$\chi_{II}^{\text{inter}}(\mathbf{q}, \omega) = -\frac{m}{\pi} \sum_s \frac{1}{8\pi} \int d\theta \left\{ \frac{F_{\mu\nu}^{s, -s}(k_s) \cos \theta}{y_s - \cos \theta + i0^+} + \frac{F_{\mu\nu}^{s, -s}(k_{-s}) \cos \theta}{\tilde{y}_s - \cos \theta + i0^+} \right\}, \quad (25)$$

where $y_s = \frac{m\omega}{k_s q} + 2s\frac{k_R}{q}$, $\tilde{y}_s = \frac{m\omega}{k_{-s} q} - 2s\frac{k_R}{q}$. Resembling the results of the intraband contribution $\chi^{\text{intra}}(\mathbf{q}, \omega)$, we can also express the results in terms of some well defined integrals

$$\chi_{II}^{\text{inter}} = -\frac{m}{4\pi} \sum_s \begin{pmatrix} 0 & \frac{s|\mathbf{q}|}{2k_s} [I_5(y_s) - I_5(\tilde{y}_s)] & 0 & 0 \\ \frac{s|\mathbf{q}|}{2k_s} [I_5(y_s) - I_5(\tilde{y}_s)] & I_5(y_s) + I_5(\tilde{y}_s) & 0 & 0 \\ 0 & 0 & I_3(y_s) + I_3(\tilde{y}_s) & -is[I_2(y_s) - I_2(\tilde{y}_s)] \\ 0 & 0 & is[I_2(y_s) - I_2(\tilde{y}_s)] & I_1(y_s) + I_1(\tilde{y}_s) \end{pmatrix}. \quad (26)$$

All of these integrations and corresponding results are given in Appendix A.

The summation of the intraband and interband contribution gives the total susceptibility

$$\chi = \chi^{\text{intra}} + \chi_I^{\text{inter}} + \chi_{II}^{\text{inter}}. \quad (27)$$

For the low- q behaviors of the collective modes, we find that the contribution of χ_{II}^{inter} is less significant. This

could be understood from that the second term of the right-hand side in Eq. (22) is much smaller than the first one in the low- q regime $|\mathbf{q}| \ll k_R$. Therefore the energy gaps of the gapped modes and the sound speed of the gapless mode are mainly determined by χ^{intra} and χ_I^{inter} . Furthermore, we will find that the gapped modes are mostly determined by the interband contribution χ_I^{inter} in the following section.

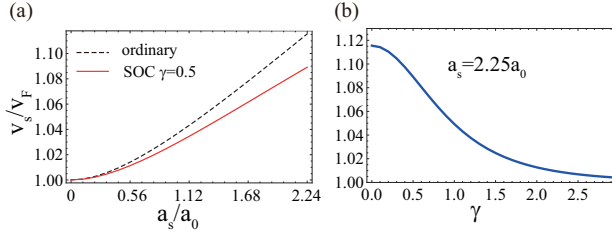


FIG. 4. (Color online) (a) The speed of zero sound as a function of s -wave scattering length. (b) The speed of zero sound as a function of the strength of SOC. The parameters used here are: the number of ^{40}K atoms is about 10^4 , $k_R = 2\pi/\lambda$ with $\lambda = 773\text{nm}$, $\gamma = 0.5$, trapping frequencies $(\omega_\perp, \omega_z) = 2\pi \times (10, 400)\text{Hz}$, and $a_s = 2.25a_0$, where a_0 is the Bohr Radius. The corresponding dimensionless interaction strength mg is about 2.5, which is less than the critical value π .

IV. COLLECTIVE MODES

In this section, we study the collective behaviors in the long wave length regime with $|\mathbf{q}| \ll k_R$ via the poles of the density and spin RPA correlation functions [46]. The susceptibility can be expanded with respect to the small dimensionless parameter $|\mathbf{q}|/k_R$.

We consider the weak SOC at first, for which we have $y_s \approx \tilde{y}_s \approx y + 2sk_R/|\mathbf{q}|$. In the long wave length limit $|\mathbf{q}| \ll k_R$, there is $|y_s|, |\tilde{y}_s| \gg 1$. In Appendix A, we give the asymptotic behaviors of the integrals in Eq. (20), (23) and (26) for $|y_s|, |\tilde{y}_s| \gg 1$. Given these asymptotic behaviors, the susceptibility in the subspace of n - s^T can be expanded to $\mathcal{O}((|\mathbf{q}|/k_R)^2)$. To study the low- q behaviors of the collective modes, it is useful to note the following behaviors of $\chi^{\mu\nu}$. If the dimensionless ratio $y = m\omega/\kappa k_F |\mathbf{q}|$ is fixed when $q \rightarrow 0$, we obtain

$$\chi_{nT} = \begin{pmatrix} \chi_{nn} & \frac{2}{\kappa} y \chi_{nn} \\ \frac{2}{\kappa} y \chi_{nn} & \frac{m}{\pi} + y^2 \chi_{nn} \end{pmatrix}, \quad |\mathbf{q}| \rightarrow 0, y \text{ fixed}, \quad (28)$$

where $\chi_{nn} = -mI_1(y)/\pi$ is the density-density element of the susceptibility matrix. The formula of χ_{nT} in the long wave length limit with y fixed holds for strong SOC. If we fix the ω when $|\mathbf{q}| \rightarrow 0$, the dimensionless parameter y tends to infinity, which leads to

$$\chi_{nT} = \frac{m}{\pi} \begin{pmatrix} 0 & 0 \\ 0 & \frac{8\gamma^2 \epsilon_F^2}{16\gamma^2 \epsilon_F^2 - \omega^2} \end{pmatrix}, \quad |\mathbf{q}| \rightarrow 0, \omega \text{ fixed}, \quad (29)$$

where the intraband has no contribution in this limit. From Eq. (28) and (29), we conclude that the solutions contain two different categories: (i) the gapless modes, which are coupled oscillations of the density and transverse spin excitations; (ii) the gapped modes, which are the oscillations of the transverse spin excitations.

The collective modes in this subspace can be determined by the poles of RPA susceptibility in Eq. (8),

which are given by

$$\det(1 + g\sigma_z \chi_{nT}) = 0. \quad (30)$$

The solutions of the real part of Eq. (30) give rise to the dispersions of the collective modes. Within the scheme of RPA, we find that the determinant $\det(1 + g\sigma_z \chi_{nT})$ will develop a non-zero imaginary part when the dispersions fall in the particle-hole continuum, which is given in Fig. 3. For this regime, the collective modes are unstable and will decay through particle-hole pairs. Substitute Eq. (28) to Eq. (30), we obtain a gapless dispersion, which is given by the solution of

$$(1 + g\chi_{nn})[1 - g(\frac{m}{\pi} + y^2 \chi_{nn})] + \frac{\gamma^2}{\kappa^2} g^2 y^2 \chi_{nn}^2 = 0. \quad (31)$$

From Eq. (28), we find that the density component is coupled with the transverse spin component. Therefore the zero sound is a coupled oscillation of the density and transverse spin excitations. There is a critical value for the interaction strength, i.e., $g_c = \frac{\pi}{m}$, above which, the SOC Fermi gas experiences a Stoner instability. In the normal state regime we have $g < g_c$. In Fig. 4 (a), we show the sound speed of this gapless mode by solving Eq. (31) numerically. For comparison, the sound speed of the ordinary Fermi liquid without SOC is shown together.

Substitute Eq. (29) to Eq. (30), we obtain one branch of gapped mode corresponding to transverse spin oscillation. The frequency at $|\mathbf{q}| = 0$ of this mode is given by the solution of

$$1 - \frac{mg}{\pi} \frac{8\gamma^2 \epsilon_F^2}{16\gamma^2 \epsilon_F^2 - \omega^2} = 0, \quad (32)$$

which yields the result

$$\Delta_T = 4\sqrt{1 - mg/2\pi\gamma\epsilon_F}, \quad (33)$$

where Δ_T is the energy gap of the transverse spin mode, $mg = \varepsilon_{int}/\varepsilon_{kin}$ is the dimensionless ratio of interaction energy and kinetic energy in 2D, which denotes the significance of interaction strength in ultracold atomic system.

Similarly, we consider susceptibility in the s^L - s^Z subspace in the limit $q \ll k_R$ and $\gamma \ll 1$. The RPA susceptibility χ_{LZ}^{RPA} is positive definite in the limit $q \rightarrow 0$ while keeping y fixed in the normal state regime. Therefore there does not exist gapless excitations in the the longitudinal and perpendicular spin subspace. In the limit $q \rightarrow 0$ while keeping ω fixed, the interband susceptibility dominates and gives rise to

$$\chi_{LZ} = \frac{m}{\pi} \begin{pmatrix} \frac{8\gamma^2 \epsilon_F^2}{16\gamma^2 \epsilon_F^2 - \omega^2} & 0 \\ 0 & \frac{16\gamma^2 \epsilon_F^2}{16\gamma^2 \epsilon_F^2 - \omega^2} \end{pmatrix}. \quad (34)$$

The poles of RPA susceptibility $\chi_{LZ}^{RPA} = \chi_{LZ}[1 - g\chi_{LZ}]^{-1}$ give rise to two branches of gapped modes corresponding to the longitudinal and perpendicular spin oscillations.

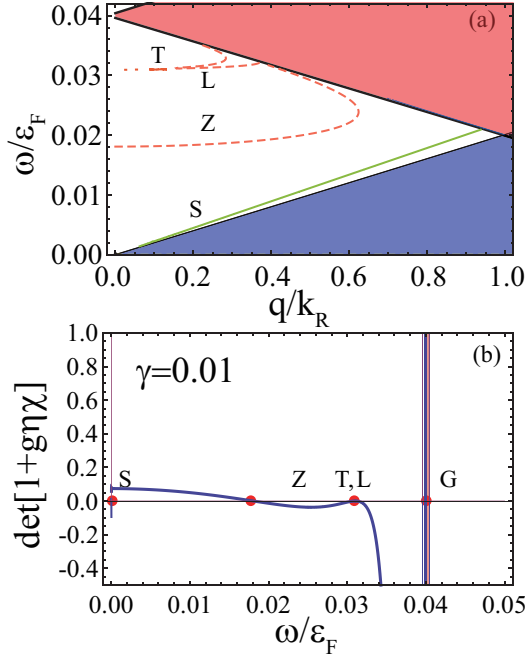


FIG. 5. (Color online) (a) The collective excitations for weak SOC with $\gamma = 0.01$. The other parameters used here are the same with Fig. 4. The transverse, longitudinal and perpendicular spin excitations are labeled by T, L and Z . S denotes the zero sound mode. (b) The corresponding graphical solutions of the energy gaps at $|\mathbf{q}| = 0$ for $\gamma = 0.01$. The energy gaps Δ_T and Δ_L for the gapped modes T and L are degenerate, and the other solutions with nearly degenerated finite energy gaps labeled by G fall in the particle-hole continuum (the narrow pink region) and are therefore damped in weak SOC regime.

The frequencies at $|\mathbf{q}| = 0$ of these two modes are given as follows

$$\Delta_L = 4\sqrt{1 - mg/2\pi\gamma\epsilon_F}, \quad (35a)$$

$$\Delta_Z = 4\sqrt{1 - mg/\pi\gamma\epsilon_F}, \quad (35b)$$

where Δ_L and Δ_Z are the energy gaps for the longitudinal spin and perpendicular spin modes respectively.

Compared with the formula of Δ_T in Eq. (33), we notice that the energy gaps for transverse spin and longitudinal spin modes are degenerate: $\Delta_T = \Delta_L$. This degeneracy could be understood generally as follows. For finite momentum of the collective excitations \mathbf{q} , the in-plane spin could be divided into transverse (s^T) and longitudinal (s^L) components relative to the direction of \mathbf{q} as defined in Sec. II. In the limit $\mathbf{q} \rightarrow 0$, the in-plane spin components s^T and s^L are not distinguishable. And therefore the susceptibility for the in-plane spin fluctuations are isotropic. As a result the corresponding energy gaps Δ_T and Δ_L equal to each other. For non-zero momentum, this degeneracy is lifted and the collective modes for s^T and s^L fluctuations have different dispersions. This argument for the degeneracy also applies to

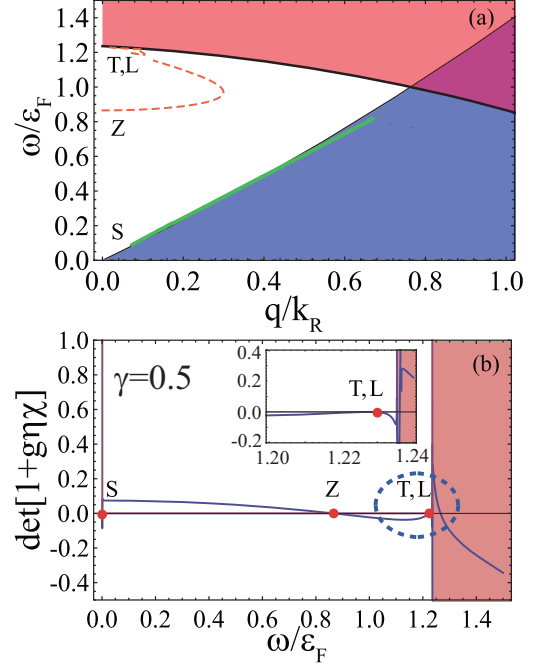


FIG. 6. (Color online) The collective excitations for strong SOC with $\gamma = 0.5$. The other parameters and the notations of these collective modes are the same with Fig. 5. We obtain one branch of gapless mode denoted as S and three branches of gapped modes denoted as T, L and Z . (b) The corresponding graphical solutions of the energy gaps at $|\mathbf{q}| = 0$ for strong SOC with $\gamma = 0.5$. The energy gaps Δ_T and Δ_L are still degenerate with values close to the edge of the interband particle-hole continuum (shown in the inset figure). The other modes falling in the particle-hole continuum (the pink region) are damped.

the case for strong SOC, which is shown explicitly in the following discussions.

In Fig. 5, we show the numerical results for collective modes and the graphical solutions of the energy gaps for weak SOC with $\gamma = 0.01$, where the gapless zero sound mode is labeled as S and the transverse, longitudinal and perpendicular spin excitations are labeled by T, L and Z respectively. In the graphical solutions shown in Fig. 5 (b), we observed several additional solutions with nearly degenerated finite energy gaps labeled by G . However, all of gapped modes G fall in the particle-hole continuum of the interband excitations and are therefore damped.

We now want to consider the collective modes for strong SOC. In the present experiments [14, 15], the typical experimental values for the dimensionless ratio γ ranges from about 0.5 to 1. Thus we need to consider the case for $\gamma \sim \mathcal{O}(1)$ based on Eq. (20), (24) and (26) in the following. The same as the case of weak SOC, the contribution from Eq. (26) is found to be negligible at the low- q regime. We give the graphical solutions for these collective excitations in Fig. 6 and the sound speed of the gapless mode with strong SOC has been shown in

Fig. 4 (b).

The transverse, longitudinal and perpendicular spin excitation T, L, Z still exist as shown in Fig. 6 and the analytical formula for the energy gap of perpendicular spin modes Δ_T , Δ_L , and Δ_Z given by (33) and (35) provide qualitative approximations with corrections about $\mathcal{O}(\gamma^2)$. The two in-plane modes T, L exist close to the edge of the interband particle-hole continuum, which is shown by the inset of Fig. 6 (b). For typical experiment parameters, the dimensionless SOC strength $\gamma \sim 0.5 - 1$ and the dimensionless interaction strength $mg = 2.5$. The numerical analysis shows that the energy gaps for the corresponding gapped modes in units of ε_F reads as $\Delta_T = \Delta_L = 3.10\gamma - 0.75\gamma^2 + \mathcal{O}(\gamma^3)$, $\Delta_Z = 1.81\gamma + 0.35\gamma^2 + \mathcal{O}(\gamma^3)$. Besides, there are several additional poles of determinant of the RPA susceptibility with finite energy gaps. Similar to the case of weak SOC, all of these modes fall in the interband particle-hole continuum (shown in Fig. 3) and are therefore damped. The sound speed of the gapless mode as a function of the strength of SOC is shown in Fig. 4 (b), which decreases as the strength of SOC is increasing. In particular, the sound speed for strong SOC can also be determined by the solutions of Eq. (31). In fact, Eq. (28) holds both for weak and strong SOC in the limit $|\mathbf{q}| \rightarrow 0$ with $m\omega/\kappa k_F |\mathbf{q}|$ kept fixed, which originates from the usual continuity equation and has been explicitly calculated above. Similar forms could be found in graphene sheets [47].

V. COMPARISONS AND DISCUSSIONS

We have noticed some previous works focused on collective modes in various solid and ultracold atomic systems, such as the two dimensional electron gas (2DEG) in semi-conductors [48–53], the A phase and B phase in Helium-3 [54, 55]. Furthermore, the surface states of 3D topological insulators are known as the helical liquid, which can be considered as the system with only the Rashba Hamiltonian. The collective modes in this helical liquid with Coulomb interactions or the repulsive short-ranged interactions have been explored in Ref. [56]. As a comparison and conclusion, we list these main results for the various systems in Table. I.

For Coulomb interaction which is listed in the first column of Table. I, the collective modes have the same dispersion relations $\omega \propto \sqrt{q}$ in 2D, since the poles of the RPA susceptibility just depend on the bare density-density susceptibility χ_{nn} , which are solved by

$$1 + V_C(q)\chi_{nn} = 0, \quad (36)$$

where $V_C(q)$ is the Coulomb interaction vertex in 2D.

In contrast to the Coulomb interaction, the s -wave interaction has two dramatically different features. First, the force range is short. Secondly, the s -wave interaction can be decomposed into the density and spin channels

[30]. The interaction is repulsive in the density channel while attractive in the spin channel. Both of these two aspects have significant influences on the low- q behaviors of the collective modes. The results are listed in the second column of Table I, which are classified as following:

(1). *Ordinary Fermi liquid*— In the absence of SOC, the bare density and spin susceptibility for the ordinary Fermi liquid is $\chi_{nn}I_{4 \times 4}$. The fluctuation of spin channel is suppressed because the interaction vertex for the spin susceptibility χ_{ss} is negative. The RPA equation $1 + g\chi_{nn} = 0$ gives rise to a linear dispersion relation, with the sound velocity $v_s > v_F$. The short range of the s -wave interaction is essential for the excitation of this mode.

(2). *Helical liquid*— Similarly, the collective modes in the helical liquid with short-ranged interaction are also gapless. However, in the helical liquid, the zero sound can be damped even for a repulsive interaction which is larger than the critical value U_c as shown in Table I. In fact, due to the a operator identity, $\mathbf{j}(\mathbf{x}) = v_f \mathbf{S}(\mathbf{x}) \times \hat{\mathbf{z}}$, which relates the density current to the in-plane component of the spin on the surface [56], the spin and density fluctuations are intrinsically coupled. The effectively attractive interaction in the spin channel results in the damping of sound mode.

(3). *SOC Fermi gas*— The Hamiltonian of SOC Fermi gas includes both the quadratic term $\mathbf{k}^2/2m$ and the Rashba SOC term. The Fermi momentum k_F and recoil momentum k_R provide two scales for the system. The significance of the SOC is characterized by the dimensionless ratio $\gamma = k_R/k_F$. When we consider the gapped modes with energy gaps of $\mathcal{O}(\gamma\varepsilon_F)$, the contribution of interband dominates while the intraband is well suppressed. We obtain three branches of undamped gapped modes bellow the interband particle-hole continuum corresponding to the spin oscillations (see Fig. 5 and 6). For the limit $\gamma \rightarrow 0$, the gapped modes T, L, Z bellow the interband continuum will fall in the particle-hole continuum and are therefore damped. While for strong SOC limit $\gamma \rightarrow \infty$, the energy gaps are much higher than the Fermi energy and are not observable in the low energy scales. These two limits coincide with the results of the ordinary Fermi liquid and the helical liquid. Besides, we also obtained one branch of gapless collective excitation, i.e., the zero sound with linear dispersion $\omega \propto v_F q$, which is a combined oscillation of density and transverse spin.

VI. EXPERIMENTAL SIGNATURES AND SUMMARIES

We have shown the behaviors of collective modes in the long wave length limit with SOC and repulsive s -wave interaction. Recently, the SOC in Fermi gas has been realized with ^{40}K atoms [14] and ^6Li atoms [15]. In their experiments, the equal weight combination of Rashba-type and Dresselhaus-type SOC is realized. This is the first step towards the realization of pure type of SOC

TABLE I. Comparisons of the ordinary Fermi liquid, SOC Fermi liquid, and helical liquid. Both RPA results for the charged cases and the neutral cases with s -wave interaction are listed.

	Coulomb interaction	s -wave interaction
ordinary Fermi liquid	$\omega = \sqrt{\frac{2\pi n e^2 q}{m\epsilon}}^*$	$\omega = \frac{1+\pi/mg}{\sqrt{(1+\pi/mg)^2-1}} v_F q$
SOC Fermi liquid	$\omega = \sqrt{\frac{2\mathcal{D}q}{\epsilon}}^{**}$	i): gapless $\omega = v_s q, v_s > v_F$. ii): gapped $\begin{cases} \Delta_T = \Delta_L = 4\sqrt{1-mg/2\pi\gamma\epsilon_F}, \\ \Delta_Z = 4\sqrt{1-mg/\pi\gamma\epsilon_F}. \end{cases}$
Helical liquid [56]	$\omega = \mu\sqrt{\frac{\epsilon^2 q}{4\epsilon_d \pi \mu}}$	$\omega = v_F q(1 + 8g^2/g_c^2), g/g_c \rightarrow 0,$ $\omega = v_F q\sqrt{\frac{7}{4}\frac{g}{g-g_c}}, g/g_c \rightarrow 1.$

* Here ϵ is the dielectric constant of the ordinary Fermi liquid, and the ϵ in the second and third row is the dielectric constant of semiconductors with SOC and the bulk of the topological insulator, respectively. n is the density of the charged particle [45].

** Here \mathcal{D} is the Drude weight, which is connected with the spin susceptibility [45].

experimentally. In this work, we focus on the Rashba-type SOC, and the Dresselhaus-type SOC is presented in Appendix B, which is demonstrated to give the same results as the Rashba SOC for collective behaviors. The short-ranged repulsive s -wave interaction can be achieved on the upper branch of a Feshbach resonance, where there are uncondensed Fermi gases in the absence of molecule formation [16]. The repulsive Fermi gas is metastable for observation when it is far away from the resonant regime, and has been successfully reached in the recent experiment [17].

We choose the following typical experimental parameters for quasi-2D system considered here. We consider about 10^4 ^{40}K atoms in a pancake-shaped harmonic potential with the trapping frequencies $2\pi \times (10, 10, 400)\text{Hz}$ along the $(\hat{x}, \hat{y}, \hat{z})$ direction. The system size is estimated as $(37.8, 37.8, 5.98)\mu\text{m}$. The strength of SOC γ is chosen as 0.5 and a_s is tuned to $2.25a_0$ (within the normal state regime) with Feshbach resonance. For the parameters used here, we estimate that the zero sound velocity is about $1.09v_F$, and the energy gaps for the gapped modes are $\Delta_T = \Delta_L = 1.23\epsilon_F$ and $\Delta_Z = 0.86\epsilon_F$. The Fermi velocity v_F is about 0.028m/s and the Fermi energy $\epsilon_F = \hbar \times 33.36\text{kHz}$. To observe these dynamical oscillations in experiment, we suggest the following methods. (i): The gapless mode could be excited by a short laser pulse focused near the center of the trap [57]. The oscillation could be detected via the spatially resolved images of the coupled density and transverse spin perturbances propagating through the trapped atomic cloud [58]. (ii): The gapped modes are spin oscillations, which are actually the oscillations of the internal hyperfine states of atoms. The oscillations could be excited via a two-photon drive, and traced out through the state-selective absorption imaging method and repeating the experiment for many values of evolution time [58, 59].

In summary, we studied the SOC effect on the low- q behaviors of collective modes in Fermi gas with repulsive s -wave interaction. There are two categories of collective modes in this system. One branch has gapless dispersion, known as the zero sound. In SOC system, the density oscillation is coupled with the spin oscillation for this mode. The other three branches are collective excitations with finite energy gaps. We calculated the sound speed of the gapless mode and the energy gaps of the gapped modes, and also estimated their values for typical experimental parameters. In addition, the repulsive s -wave interaction has a profound significance. In the presence of Coulomb interaction, the collective modes for ordinary Fermi liquid, SOC Fermi gas, and helical liquid have the same dispersion relation as $\omega \sim \sqrt{q}$ in 2D. In contrast, the s -wave interaction leads to fundamentally different phenomena, such as the presence of linear dispersion of the zero sound and the gapped modes. The study on the collective modes of the SOC repulsive Fermi gas indicates some novel behaviors due to the presence of SOC, and also might have the immediate applicability to experimental study of the SOC Fermi gases in the upper branch of the energy spectrum.

ACKNOWLEDGMENTS

We acknowledge helpful discussions with Han Pu, and Congjun Wu. S. S. Zhang, X. L. Yu, and W. M. Liu were supported by the NKBRSCF under grants Nos. 2011CB921502, 2012CB821305, 2009CB930701, 2010CB922904, NSFC under grants Nos. 10934010, 11228409, 61227902 and NSFC-RGC under grants Nos. 11061160490 and 1386-N-HKU748/10. J. Ye was supported by NSF-DMR-1161497, NSFC-11074173,

11174210, Beijing Municipal Commission of Education under Grant No. PHR201107121, at KITP was supported in part by the NSF under grant No. PHY11-25915.

Appendix A: EVALUATIONS OF SOME RELEVANT INTEGRALS

When we calculated the density and spin susceptibility in Sec. III, we met with some integrals of the azimuthal angle θ , such as $I_0, I_1, I_2, I_3, I_4, I_5$. Since they have the similar structures, we evaluate them in this Appendix. The definitions of these integrations are listed as below:

$$I_0(y) = \int \frac{d\theta}{2\pi} \frac{1}{y - \cos\theta + i0^+}, \quad (\text{A1})$$

$$I_1(y) = \int \frac{d\theta}{2\pi} \frac{\cos\theta}{y - \cos\theta + i0^+}, \quad (\text{A2})$$

$$I_2(y) = \int \frac{d\theta}{2\pi} \frac{\cos^2\theta}{y - \cos\theta + i0^+}, \quad (\text{A3})$$

$$I_3(y) = \int \frac{d\theta}{2\pi} \frac{\cos^3\theta}{y - \cos\theta + i0^+}, \quad (\text{A4})$$

$$I_4(y) = \int \frac{d\theta}{2\pi} \frac{\sin^2\theta}{y - \cos\theta + i0^+}, \quad (\text{A5})$$

$$I_5(y) = \int \frac{d\theta}{2\pi} \frac{\cos\theta \sin^2\theta}{y - \cos\theta + i0^+}. \quad (\text{A6})$$

At first we note that if $|y| < 1$, these integrals have a non-zero imaginary part; if $|y| > 1$, these integrals are real. This can be seen from the following calculation. This property results in the damping of the collective modes in the particle-hole excitation continuum.

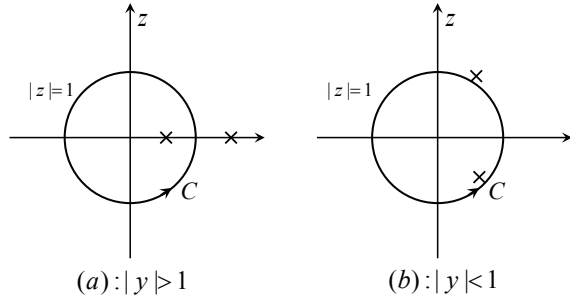


FIG. 7. Schematic of the integral path and the poles of the integrand functions. The location of the poles are different for $|y| > 1$ and $|y| < 1$, which are shown in (a) and (b) respectively.

These integrals can be mapped into the integrals in the complex- z plane with a transformation $z = e^{i\theta}$. The integral path C is the unit circle with the center at $(0, 0)$. We show the integral path and gives a schematic of the poles of the integrand function for $|y| > 1$ and $|y| < 1$ in Fig. 7. With the theorem of residue, these integrals are

evaluated straightforwardly:

$$I_0(y) = \frac{\text{sign}(y)}{\sqrt{y^2 - 1}} \Theta(|y| - 1) - \frac{i}{\sqrt{1 - y^2}} \Theta(1 - |y|), \quad (\text{A7})$$

$$I_1(y) = -1 + \frac{|y|}{\sqrt{y^2 - 1}} \Theta(|y| - 1) - \frac{iy}{\sqrt{1 - y^2}} \Theta(1 - |y|), \quad (\text{A8})$$

$$I_2(y) = -y + \frac{y|y|}{\sqrt{y^2 - 1}} \Theta(|y| - 1) - i \frac{y^2}{\sqrt{1 - y^2}} \Theta(1 - |y|), \quad (\text{A9})$$

$$I_3(y) = -\frac{1}{2} - y^2 + \frac{y^2|y|}{\sqrt{y^2 - 1}} \Theta(|y| - 1) - \frac{iy^3}{\sqrt{1 - y^2}} \Theta(1 - |y|), \quad (\text{A10})$$

$$I_4(y) = y - \text{sign}(y) \sqrt{y^2 - 1} \theta(|y| - 1) - i \sqrt{1 - y^2} \theta(1 - |y|), \quad (\text{A11})$$

$$I_5(y) = -\frac{1}{2} + y^2 - |y| \sqrt{y^2 - 1} \Theta(|y| - 1) - iy \sqrt{1 - y^2} \Theta(1 - |y|). \quad (\text{A12})$$

where $\Theta(x)$ is the unitstep function. When we were exploring the analytical expressions of the susceptibility in Eq. (20), (23) and (26) in the region $q \ll k_R$, we used the asymptotic behaviors at $|y| \rightarrow \infty$:

$$I_0(y) \simeq \frac{1}{y}, I_1(y) \simeq \frac{1}{2y^2}, I_2(y) \simeq \frac{1}{2y}, \\ I_3(y) \simeq \frac{3}{8y^2}, I_4(y) \simeq \frac{1}{2y}, I_5(y) \simeq \frac{1}{8y^2}. \quad (\text{A13})$$

Appendix B: EQUIVALENCE BETWEEN THE RASHBA SOC AND DRESSSELHAUS SOC

We start with the single particle Hamiltonian with Dresselhaus SOC [13]

$$\mathcal{H}_D = \frac{\mathbf{k}^2}{2m} + \alpha(-k_y \sigma_x - k_x \sigma_y) - \mu. \quad (\text{B1})$$

The various quantities calculated in this paper is closely based on the well-defined Feynman rules. The Feynman rules include the single particle Green's function and the interaction vertex. Within the scheme of RPA, the collective modes are determined by the poles of the RPA susceptibility, which is given by (8). It is apparent that the properties of the collective modes depends on the bare susceptibility $\chi(\mathbf{k}, \omega)$. Therefore, we want to derive

the relationships between the two types of SOC system as follows.

For the Dresselhaus-type SOC, the non-interacting Green's function and the interaction vertex reads

$$G^D(\omega, \xi_{\mathbf{k},s}) = \sum_s \frac{P_s^D}{\omega - \xi_{\mathbf{k},s} + i0^+}, \quad (\text{B2})$$

$$V_{ss';rr'}^D(\mathbf{k}, \mathbf{p}, \mathbf{q}) = g f_{ss'}^D(\theta_{\mathbf{k}}, \theta_{\mathbf{k}+\mathbf{q}}) f_{rr'}^D(\theta_{\mathbf{p}}, \theta_{\mathbf{p}-\mathbf{q}}). \quad (\text{B3})$$

where the upscript D represents the Dresselhaus-type SOC, and P_s^D is the projection operator defined as

$$P_s^D = \frac{1}{2}[1 + s(-k_y\sigma_x - k_x\sigma_y)]. \quad (\text{B4})$$

The energy spectrum of the Dresselhaus-type SOC is the same with the Rashba-type. However, the spin polarization is different from Rashba SOC, which is

$$P_s^R = \frac{1}{2}[1 + s(-k_y\sigma_x + k_x\sigma_y)]. \quad (\text{B5})$$

The trace in Eq. (10) includes an overlap factor for

the Dresselhaus case as

$$F_{sr}^{D,\mu\nu} = \text{tr} [P_s^D(\mathbf{k} - \mathbf{q}/2) \sigma_\mu P_r^D(\mathbf{k} + \mathbf{q}/2) \sigma_\nu]. \quad (\text{B6})$$

Given Eq. (B4) and (B5), the overlap factor for the two cases can be related by transformation $k_x \rightarrow -k_x, q_x \rightarrow -q_x$, while keeping the y component invariant. The bare susceptibility with Dresselhaus SOC is given by

$$\chi^{D,\mu\nu}(\mathbf{q}, \omega) = - \sum_{\mathbf{k}, s, r} F_{sr}^{D,\mu\nu} \frac{f(\xi_{\mathbf{k}-\mathbf{q}/2, s}) - f(\xi_{\mathbf{k}+\mathbf{q}/2, r})}{\xi_{\mathbf{k}-\mathbf{q}/2, s} - \xi_{\mathbf{k}+\mathbf{q}/2, r} + \omega + i0^+}. \quad (\text{B7})$$

Due to the rotation symmetry, we choose $\mathbf{q} = q\mathbf{e}_y$ for simplicity. Given the relationship between the overlap factor for Rashba SOC and Dresselhaus SOC and the rotational symmetry of the energy spectrum, we have

$$\chi^{D,\mu\nu}(q\mathbf{e}_y, \omega) = \chi^{R,\mu\nu}(q\mathbf{e}_y, \omega). \quad (\text{B8})$$

Therefore we conclude that all the properties and classification of the collective modes for the two type of SOC are all the same exactly.

-
- [1] Y. K. Kato, R. C. Myers, A. C. Gossard, and D. D. Awschalom, *Science* **306**, 1910 (2004).
 - [2] J. Wunderlich, B. Kaestner, J. Sinova, and T. Jungwirth, *Phys. Rev. Lett.* **94**, 047204 (2005).
 - [3] B. A. Bernevig, T. L. Hughes, and S. C. Zhang, *Science* **314**, 1757 (2006).
 - [4] M. König, S. Wiedmann, C. Bruene, A. Roth, H. Buhmann, L. W. Molenkamp, X. L. Qi, and S. -C. Zhang, *Science* **318**, 766 (2007).
 - [5] C. L. Kane and E. J. Mele, *Phys. Rev. Lett.* **95**, 226801 (2005).
 - [6] B. A. Bernevig and S. C. Zhang, *Phys. Rev. Lett.* **96**, 106802 (2006).
 - [7] J. D. Koralek, C. P. Weber, J. Orenstein, B. A. Bernevig, S. C. Zhang, S. Mack, and D. D. Awschalom, *Nature (London)* **458**, 610 (2009).
 - [8] F. Wilczek and A. Zee, *Proc. R. Soc. Lond. A* **392**, 45 (1984).
 - [9] F. Wilczek and A. Zee, *Phys. Rev. Lett.* **52**, 2111 (1984).
 - [10] Y. J. Lin, R. L. Compton, A. R. Perry, W. D. Phillips, J. V. Porto, and I. B. Spielman, *Phys. Rev. Lett.* **102**, 130401 (2009).
 - [11] Y. J. Lin, R. L. Compton, K. Jiménez-García, J. V. Porto, and I. B. Spielman, *Nature (London)* **462**, 628 (2009).
 - [12] Y. J. Lin, R. L. Compton, K. Jiménez-García, W. D. Phillips, J. V. Porto, and I. B. Spielman, *Nat. Phys.* **7**, 531 (2011).
 - [13] Y. J. Lin, K. Jiménez-García, and I. B. Spielman, *Nature (London)* **471**, 83 (2011).
 - [14] P. Wang, Z. Q. Yu, Z. Fu, J. Miao, L. Huang, S. Chai, H. Zhai, and J. Zhang, *Phys. Rev. Lett.* **109**, 095301 (2012).
 - [15] L. W. Cheuk, A. T. Sommer, Z. Hadzibabic, T. Yefsah, W. S. Bakr, and M. W. Zwierlein, *Phys. Rev. Lett.* **109**, 095302 (2012).
 - [16] V. B. Shenoy and T.-L. Ho, *Phys. Rev. Lett.* **107**, 210401 (2011).
 - [17] G. B. Jo, Y. R. Lee, J. H. Choi, C. A. Christensen, T. H. Kim, J. H. Thywissen, D. E. Pritchard, and W. Ketterle, *Science* **325**, 1521 (2009).
 - [18] X. L. Yu, S. S. Zhang, and W. M. Liu, arXiv:1212.0420.
 - [19] H. Hu, A. Minguzzi, X. J. Liu, and M. P. Tosi, *Phys. Rev. Lett.* **93**, 190403 (2012).
 - [20] M. J. Wright, S. Riedl, A. Altmeyer, C. Kohstall, E. R. Sanchez Guajardo, J. H. Denschlag, and R. Grimm, *Phys. Rev. Lett.* **99**, 150403 (2007).
 - [21] M. Bartenstein, A. Altmeyer, S. Riedl, S. Jochim, C. Chin, J. H. Denschlag, and R. Grimm, *Phys. Rev. Lett.* **92**, 203201 (2004).
 - [22] A. Altmeyer, S. Riedl, C. Kohstall, M. J. Wright, R. Geursen, M. Bartenstein, C. Chin, J. H. Denschlag, and R. Grimm, *Phys. Rev. Lett.* **98**, 040401 (2007).
 - [23] S. Riedl, E. R. Sánchez Guajardo, C. Kohstall, A. Altmeyer, M. J. Wright, J. H. Denschlag, R. Grimm, G. M. Bruun, and H. Smith, *Phys. Rev. A* **78**, 053609 (2008).
 - [24] J. Kinast, S. L. Hemmer, M. E. Gehm, A. Turlapov, and J. E. Thomas, *Phys. Rev. Lett.* **92**, 150402 (2004).
 - [25] J. Kinast, A. Turlapov, and J. E. Thomas, *Phys. Rev. A* **70**, 051401(R) (2004).
 - [26] S. Stringari, *Europhys. Lett.* **65**, 749 (2004).
 - [27] S. Nascimbène, N. Navon, K. J. Jiang, L. Tarruell, M. Teichmann, J. McKeever, F. Chevy, and C. Salomon, *Phys. Rev. Lett.* **103**, 170402 (2009).
 - [28] J. Y. Zhang, S. C. Ji, Z. Chen, L. Zhang, Z. D. Du, B. Yan, G. S. Pan, B. Zhao, Y. J. Deng, H. Zhai, S. Chen, and J. W. Pan, *Phys. Rev. Lett.* **109**, 115301 (2012).
 - [29] Z. Chen and H. Zhai, *Phys. Rev. A* **86**, 041604(R) (2012).
 - [30] G. D. Mahan, *Many-Particle Physics* (Plenum, New York, 1990).
 - [31] I. M. Lifshitz, *Sov. Phys. JETP* **11**, 1130 (1960).

- [32] F. Sun, X. L. Yu, J. Ye, H. Fan, and W. M. Liu, arXiv:1112.1852.
- [33] N. F. Mott and H. S. W. Massey, *Theory of Atomic Collisions* (Oxford University Press, London, 1965), 3rd ed.
- [34] A. Messiah, *Quantum Mechanics* (Wiley, New York, 1962).
- [35] E. Braaten and H. W. Hammer, Phys. Rep. **428**, 259 (2006).
- [36] T. Köhler, and K. Góral, Rev. Mod. Phys. **78**, 1311 (2006).
- [37] C. Chin, R. Grimm, P. J. and E. Tiesinga, Rev. Mod. Phys. **82**, 1225 (2010).
- [38] S. Inouye, M. R. Andrews, J. Stenger, H.-J. Miesner, D. M. Stamper-Kurn, and W. Ketterle, Nature (London) **392**, 151 (1998).
- [39] P. Courteille, R. S. Freeland, D. J. Heinzen, F. A. van Abeelen, and B. J. Verhaar, Phys. Rev. Lett. **81**, 69 (1998).
- [40] J. L. Roberts, N. R. Claussen, J. P. Burke, C. H. Greene, E. A. Cornell, and C. E. Wieman, Phys. Rev. Lett. **81**, 5109 (1998).
- [41] V. Vuletić, A. J. Kerman, C. Chin, and S. Chu, Phys. Rev. Lett. **82**, 1406 (1999).
- [42] B. A. Bernevig, X. Yu, and S. C. Zhang, Phys. Rev. Lett. **95**, 076602 (2005).
- [43] J. R. Schrieffer, X. G. Wen, and S. C. Zhang, Phys. Rev. B **39**, 11663 (1989).
- [44] G. H. Chen and M. E. Raikh, Phys. Rev. B **59**, 5090 (1999).
- [45] A. Agarwal, S. Chesi, T. Jungwirth, J. Sinova, G. Vignale, and M. Polini, Phys. Rev. B **83**, 115135 (2011).
- [46] J. W. Negele and H. Orland, *Quantum Many-Particle Systems* (Addison-Wesley, New York, 1988).
- [47] A. Principi, M. Polini, and G. Vignale, Phys. Rev. B **80**, 075418 (2009).
- [48] T. Das, Phys. Rev. Lett. **109**, 246406 (2012).
- [49] H. Chen, Y. Zhu, and S. Zhou, Phys. Rev. B **36**, 8189 (1987).
- [50] J. C. Ryan, Phys. Rev. B **43**, 4499 (1991).
- [51] D. Gammon, B. V. Shanabrook, J. C. Ryan, and D. S. Katzer, Phys. Rev. B **41**, 12311 (1990).
- [52] S. M. Badalyan, A. Matos-Abiague, G. Vignale, and J. Fabian, Phys. Rev. B **79**, 205305 (2009).
- [53] G. F. Giuliani and G. Vignale, *Quantum Theory of the Electron Liquid* (Cambridge University Press, Cambridge, 2005).
- [54] K. Maki, J. Low Temp. Phys. **24**, 755 (1976).
- [55] C. H. Aldrich III, C. J. Pethick, and D. Pines, Phys. Rev. Lett. **37**, 845 (1976).
- [56] S. Raghu, S. B. Chung, X. L. Qi, and S. C. Zhang, Phys. Rev. Lett. **104**, 116401 (2010).
- [57] A. Recati, P. O. Fedichev, W. Zwerger, and P. Zoller, Phys. Rev. Lett. **90**, 020401 (2003).
- [58] J. M. McGuirk, H. J. Lewandowski, D. M. Harber, T. Nikuni, J. E. Williams, and E. A. Cornell, Phys. Rev. Lett. **89**, 090402 (2002).
- [59] H. J. Lewandowski, D. M. Harber, D. L. Whitaker, and E. A. Cornell, Phys. Rev. Lett. **88**, 070403 (2002).